Biosensors and Bioelectronics 127 (2019) 200–206

Contents lists available at ScienceDirect

Biosensors and Bioelectronics

journal homepage: www.elsevier.com/locate/bios

Conical nanofluidic channel for selective quantitation of melamine in combination with β-cyclodextrin and a single-walled carbon nanotube

Zhipeng Xie[a,b], Jinlong Lei[b], Mingfeng Yang[b], Youji Li[c], Xinhua Geng[b], Simin Liu[a,*], Jiahai Wang[b,*]

[a] Institute of Advanced Materials and Nanotechnology, School of Chemistry and Chemical Engineering, Wuhan University of Science and Technology, Wuhan 430081, China
[b] School of Chemistry and Chemical Engineering, Guangzhou University, Guangzhou 510006, China
[c] Key Laboratory of Mineral Cleaner Production and Exploit of Green Functional Materials in Hunan Province, Jishou University, 416000, China

ARTICLE INFO

Keywords:
Conical nanofluidic channel
Single-walled carbon nanotubes (SWNTs)
β-cyclodextrin (β-CD)
Melamine detection

ABSTRACT

Amine group-bearing small molecules tend to adsorb onto the nanochannel surfaces, which degrades the efficiency of nanochannel sensors. In this study, we utilized host-guest knowledge to eliminate the influence of excessive small molecules. In combination with single-walled carbon nanotubes (SWNTs), β-cyclodextrin (β-CD) provided an excellent sensing performance for the conical nanochannel coated with polyethyleneimine (PEI) and zirconium ion (Zr^{4+}). By taking detection of melamine as a prototype, the as-prepared nanochannel could selectively detect melamine-elicited double-stranded DNA (dsDNA). Both excessive melamine and single-stranded DNA were removed via the addition of β-CD and SWNTs. The nanochannel sensing platform for the detection of melamine has a detection limit of as low as 4.3 nM with a suitable sensitivity, an excellent reproducibility and stability. Therefore, it is highly promising that a nanochannel sensor based on ion current rectification (ICR) can be used to detect other possible targets.

1. Introduction

Melamine (2,4,6-triamino-1,3,5-triazine, MEL), a triazine analogue with three amino groups, is widely employed for the synthesis of paints, plastics, adhesives, and other industrial applications (Sun et al., 2010; Liang et al., 2011; Guo et al., 2014). However, adding melamine to dairy products to increase the total nitrogen content is illegal (Ai and Lu, 2009; Huang et al., 2011; Wang et al., 2012), and could induce human renal pathology or even death (especially newborns) (Zhu et al., 2009a; Wang et al., 2015a, 2015b; Lee et al., 2011; Han et al., 2012).

Various analytical methods have thus been employed for melamine quantification, such as high-performance liquid chromatography (HPLC) (Ahmad et al., 2016; Ge et al., 2015; Wang et al., 2016), hyphenated mass spectrometry methods (Chen et al., 2015; Domingo et al., 2015; Rani et al., 2014; Zhao and Chen, 2016), surface enhanced Raman spectroscopy (SERS) (Giovannozzi et al., 2014; Rajapandiyan et al., 2015; Zhuang et al., 2016), near-infrared spectroscopy (NIR)/mid-infrared spectroscopy (MIR) (Balabin and Smirnov, 2011; Huang et al., 2015; Wu et al., 2016), enzyme-linked immunosorbent assay (ELISA) (Li et al., 2013; Xie et al., 2015a), capillary electrophoresis (CE) (Ji et al., 2014; Kong et al., 2014), electrochemiluminescence (Guo et al., 2011), and chemiluminescence (Zhang et al., 2011). Admittedly, these reported methods have made undeniable progress. However, for on-site applications, time-consuming, bulky and costly equipment that requires highly trained operators is not suitable. Thus, it is necessary to determine a simple, reliable and fast method for on-site melamine detection. To achieve the abovementioned goal, detection methods based on miniaturized nanodevices are highly desirable (Bai et al., 2018; Chen et al., 2017; Diao et al., 2018; Hanson et al., 2017; Idili et al., 2017). As one of the biomimetic nanodevices, solid-state nanofluidic channels have received widespread attention and have been considered to be very meaningful sensor platforms due to their relative stability and easy modification.

Among the applications of nanochannels, methods mainly focus on resistive-pulse sensing (RPS) (Beamish et al., 2017; Hu et al., 2018; Lin et al., 2017a; Lin et al., 2017b) and ion-current rectification (ICR) (Boussouar et al., 2017; Qian et al., 2018; Shang et al., 2017; Wang et al., 2018b). However, to be an ideal RPS method, precisely controllable pore sizes and lengths are required (Yin et al., 2017; Zhu et al., 2018b). It is very challenging and time consuming to fabricate a pore with a size suitable for small molecule detection. Fortunately, sensors based on ICR do not put such strict requirements on the opening

* Corresponding authors.
E-mail addresses: liusimin@wust.edu.cn (S. Liu), jiahaiwang@gzhu.edu.cn (J. Wang).

https://doi.org/10.1016/j.bios.2018.12.020

Available online 16 December 2018
0956-5663/

diameter of the nanochannel. Furthermore, the dynamic detection range of ICR sensors can be adjusted by manipulating the ICR. More encouragingly, much progress has been made during the construction of ICR sensors in recent years. Conventionally, the selectivity of ICR sensors has been achieved by immobilizing the probes on the nanochannel surface (Xie et al., 2015b; Liao et al., 2017; Niu et al., 2018). Surface modifications with probes elicit drastic environmental changes, including steric hindrance, hydrophobicity and charge, and the consequential crowded environments hinder the further efficiency of their interaction with targets. Later, ICR sensors without probe immobilization was established, which can still guarantee an excellent selectivity and a wide detection range (Guo et al., 2012; Zhai et al., 2014).

However, one recent dilemma has been that small molecules with amino groups, such as melamine, incline to adsorb onto the metal-ion-treated nanochannel surface (Zhang et al., 2015). To ensure the feasibility and expand the universality of sensors, it is quite urgent to determine an effective method to eliminate the interference of small molecules. It is worth mentioning that supramolecular have the potential to be significant candidates as shielding agents due to their ability to selectively recognize small molecules though the host-guest interaction. Several macrocyclic molecules with a hydrophobic cavity, such as cyclodextrin (Chen et al., 2018; Creamer et al., 2018; Li et al., 2018; Nagy et al., 2018), cucurbituril (Wang et al., 2018a; Zhou et al., 2018; Zhu et al., 2018a), and pillararene (Chi et al., 2015; Ogoshi et al., 2016; Sun et al., 2016), have been found to bind amine-bearing molecules. Results for this type of host-guest system open considerable opportunities for advancing nanochannel sensors. β-CD has been explored as a naturally occurring host macromolecule with specific molecular structures that contain a hydrophobic internal cavity and a hydrophilic external surface. Because of the combination of electrostatic, van der Waals forces, hydrogen bonding and hydrophobic interactions, β-CD is well known for forming an inclusion complex with various guest molecules in supramolecular chemistry, such as small molecules, cationic or anionic guests, proteins, and polymer chains (Hardy et al., 2018; Jiang et al., 2018; Song et al., 2018; Xue et al., 2016; Yang et al., 2018; Zheng et al., 2018). The aforementioned advantageous host-guest interaction exerted in β-CD can be utilized for the effective sensing of melamine.

Herein, we demonstrate a smart conical nanofluidic channel modified with PEI and Zr^{4+} that possesses sensitive and selective recognition of melamine with the help of a melamine aptamer, SWNTs and β-CD as illustrated in Scheme 1. The presence of melamine could produce stable triple hydrogen-bonding with thymine (T-M-T) (Zeng et al., 2012), and the SWNTs are effective in removing free single-stranded (ssDNA) via electrostatic adsorption (Zhang et al., 2010a; Zhang et al., 2010b). The nanochannel modified with PEI/Zr^{4+} can be used to indirectly detect melamine by quantitatively detecting the dsDNA concentration. Zr^{4+} is an ideal candidate for immobilizing or detecting biomolecules with phosphate groups because of its strong affinity for phosphate (Fang et al., 2011; Meng et al., 2012; Qi et al., 2013). Meanwhile, β-CD can be added to shield the detection system from the interference of free melamine and other analogues via the host-guest interaction (Stanly John Xavier, 2014). In this way, the artificial nanochannel biosensor exhibits an ultratrace recognition capability of melamine of approximately 4.3 nM. Additionally, the platform has an excellent stability and selectivity. More importantly, the fabricated sensing system has the potential to become a universal platform for the detection of various targets simply by adjusting the supramolecular species and sequence of the aptamer template.

2. Experimental

2.1. Materials and reagents

Formic acid (HCOOH), sodium hydroxide (NaOH), hydrochloric acid (HCl), potassium chloride (KCl), melamine, β-Cyclodextrin (β-CD), tris(hydroxymethyl)aminomethane and zirconium acetate were purchased from Aladdin Reagent Co. Copper chloride ($CuCl_2$), zinc chloride ($ZnCl_2$), iron(III) chloride ($FeCl_3$), magnesium sulphate anhydrous ($MgSO_4$), calcium chloride ($CaCl_2$), ascorbic acid (Vc), glucose and cyanuric acid were purchased from Sinopharm Chemical Reagent Co., Ltd. Single-walled carbon nanotubes (SWNTs) and polyethyleneimine (M_w = 25000, branched PEI) were purchased from Sigma-Aldrich. All chemicals were at least analytical grade. DNA oligonucleotides were synthesized from Sangon Biotechnology Co., Ltd. (Guangzhou, China). The melamine binding aptamer is 5′-TTTT TTTT TTTT TTTT TTTT TTTT TTTT TTTT-3′. The FAM-labelled melamine aptamer is 5′- TTTT TTTT TTTT TTTT TTTT TTTT TTTT TTTT TTTT-FAM-3′. Oligonucleotides were stored at − 20 °C and dissolved in Tris–HCl buffer (10 mM, pH = 7.4) before use. The chemical solutions

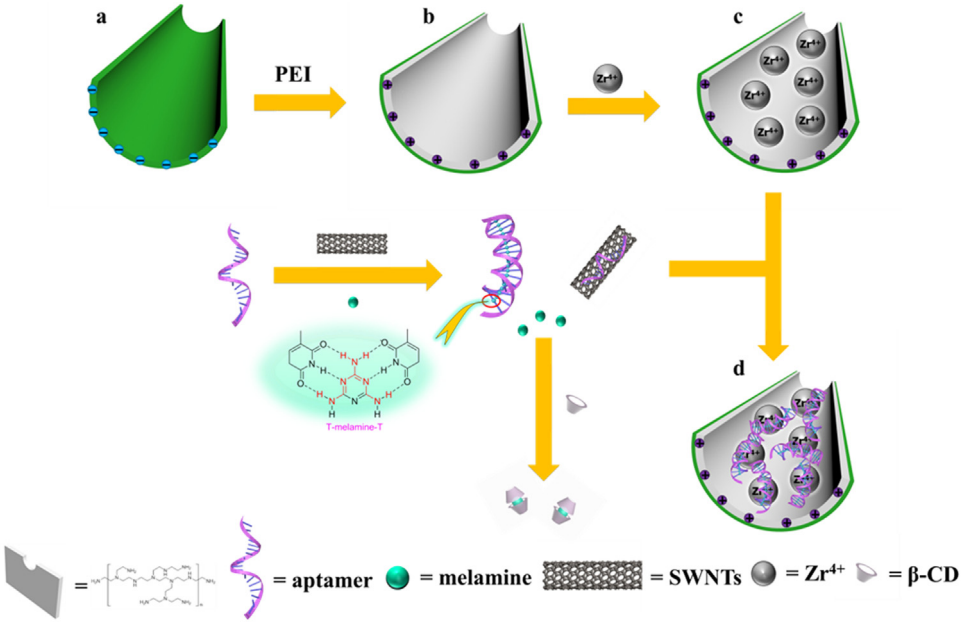

Scheme 1. Schematic description of the PEI–Zr^{4+} modified conical nanofluidic channel in different states. (a) Unmodified state after etching; (b) PEI-modified state; (c) PEI-Zr^{4+} modified state; (d) the SWNTs removing the excess ssDNA and dsDNA adsorbed by the PEI-Zr^{4+}-modified nanochannel.

were prepared in Milli-Q water (18.2 MΩ). Current-voltage curves were measured using a Keithley 6487 picoammeter (Keithley Instruments, Cleveland, OH).

2.2. Nanochannel fabrication and chemical modification

A single conical nanochannel was prepared using an asymmetric track-etch technique on a 12-μm-thick polyethylene terephthalate (PET) membrane. Before the chemical etching process, the PET membrane was further subjected to UV light (exposure to both sides for 60 min at a wavelength of 365 nm). To obtain the conical nanochannel, the PET film was folded between two chambers of a custom-designed etching cell. One side of the film was etched by an etching solution (6 M NaOH), whereas the other side was etched by stopping solution (1 M HCOOH + 1 M KCl) at 60 °C. Then, a voltage of 1 V was applied across the membrane. The etching process was stopped at a desired current value that corresponds to a certain tip diameter; then, etching was stopped. The etching solution was removed, and the stop solution was added to the pool quickly. After chemical etching, the membrane was immerged in Milli-Q water (18.2 MΩ) over night to remove residual salts. Multi-tracked PET membranes (1×10^6 tracks of cm^{-2}) were prepared as described above. After chemical etching, carboxyl groups were generated on the nanochannel surface. An aqueous solution of PEI (1% wt) was placed on the tip side of the conical nanochannel for 1 h, which could be modified on the PET surface via electrostatic adsorption. Then, an aqueous solution of zirconium acetate (8% wt) was placed on the tip side for 30 min.

2.3. Characterization

Melamine-mediated formation of the dsDNA complex was determined by UV–vis absorption spectra and CD spectra. UV–vis absorption spectra, and CD spectra were obtained with a UV-2550 spectrophotometer (Shimadzu, Japan) and a CD-250 Chirascan-plus spectrophotometer (Applied Photophysics Limited, U.K.), respectively. A Philips XL30-ESEM scanning electron microscop (SEM) was used to characterize the features of the nanochannel samples at an acceleration voltage of 5 kV. X-ray photoelectron spectra (XPS) were obtained to characterize the PET membrane before and after modification. XPS data were obtained with an EscaLab 250xi electron spectrometer from VG Scientific using 300 W Al Kα radiation.

2.4. Ion current measurement

Ion currents were measured by a Keithley 6487 picoammeter (Keithley Instruments, Cleveland, OH). A pair of Ag/AgCl electrodes was placed in two sides of the conductivity cell to apply a transmembrane potential across the nanochannel. Each current-voltage curve was measured by scanning the voltage from –1–1 V across the nanochannel membrane that was sandwiched between two chambers, and both chambers were filled with a buffering solution. All the sample solutions with melamine, β-CD, the aptamer and SWNTs were prepared in a buffering solution (100 mM KCl and 10 mM Tris-HCl at pH = 7.4). All measurements were conducted at room temperature, and each test was repeated three times to obtain the average value at different voltages. The error bars were obtained from three repeated measurements.

2.5. Validation of the feasibility of the ICR biosensor

To explore the effect of melamine on the PEI/Zr^{4+}-modified nanochannel, a series of different concentrations of melamine (100 nM, 200 nM, 1 μM, 5 μM, and 10 μM) were initially added on the tip side of the conical nanochannel. A scanning triangle voltage signal from − 1 V to 1 V with a 40 s period was selected in order to measure the I–V curves. Then, to obtain the shielding effect of β-CD on melamine in the nanofluidic channel, solutions of 1 mM β-CD and different concentrations of melamine were mixed for 30 min. The resulting solution was then used as the electrolyte for the current-voltage measurement.

2.6. Determination of melamine

First, to induce duplex formation, different concentrations of melamine (100 μL from 200 nM to 50 μM) were mixed with binding aptamer (100 μL, 2 μM) in a centrifuge tube for 1 h at room temperature. Next, β-CD (100 μL, 10 mM) was added for another 30 min to shield adsorption of excess melamine on the nanochannel surface. Then, SWNTs (100 μL, 500 μg/mL) was added to eliminate the interference from ssDNA; we then waited for 30 min. Afterwards, the resulting solution was diluted to 1 mL with the electrolyte solution. The current-voltage curve through the PEI/Zr^{4+} modified nanofluidic channel was obtained by scanning the voltage from −1 V to 1 V across the polymer membrane. (Experimental conditions: T-rich ssDNA of 200 nM, a buffering solution of 100 mM KCl and 10 mM tris-HCl at pH = 7.4, SWNTs of 50 μg/mL, 1 mM of β-CD; the total volume was 1 mL).

2.7. Selectivity

By employing analogues in the sensing platform, the specificity of the proposed strategy was assessed. Eight different interfering substances were used, including Cu^{2+}, Zn^{2+}, Fe^{3+}, Mg^{2+}, Ca^{2+}, ascorbic acid (Vc), glucose and cyanuric acid, to examine the selectivity of the strategy at a concentration of 100 nM, and we used the same experimental process as the one shown for melamine detection.

2.8. Melamine assay of a real sample

Liquid milk was pretreated according to a previous report (Hu et al., 2017). The recovery was validated in liquid milk samples using melamine at various concentrations. The possibility and reliability of the application in practice were established by evaluating the recovery rate in actual samples. For standard samples (20, 50 and 100 nM), the liquid milk samples were spiked with a range of concentrations of melamine. The electrochemical detection procedures were identical as those described above.

3. Results and discussion

3.1. I-V characterization of the chemically-modified nanochannel

As shown in Fig. S2A, a better ICR was obtained after subsequent modification of the nascent nanochannel with a branched PEI polymer and Zr^{4+} ions. The highest ICR expanded the detection range and enhanced the sensitivity of the as-prepared biomimetic sensor. The successful modification of the nanochannel is due to the presence of the carboxyl group on the nanochannel surface after chemical etching. Positively charged PEI could be easily adsorbed onto the nanochannel surface due to the electrostatic interaction, leading to the upward curve. In the buffered solution (100 mM KCl, 10 mM Tris-HCl with pH = 7.4), the nascent nanochannel surface had many negatively charged carboxyl groups; thus, the corresponding ion rectifying curve was a downward nonlinear curve (Fig. S2A, black curve). After electrostatic adsorption of the branched PEI polymer, the current at positive voltage intensively increased and was accompanied by an obvious ICR, which was attributed to the protonation of the amino groups (Fig. S2A, red curve). Further adsorption of the positively charged Zr^{4+} slightly enhanced the ICR of the conical nanofluidic channel (Fig. S2A, blue curve).

3.2. Validation of the feasibility of the ICR biosensor

To validate the feasibility of the ICR biosensor, we explored the

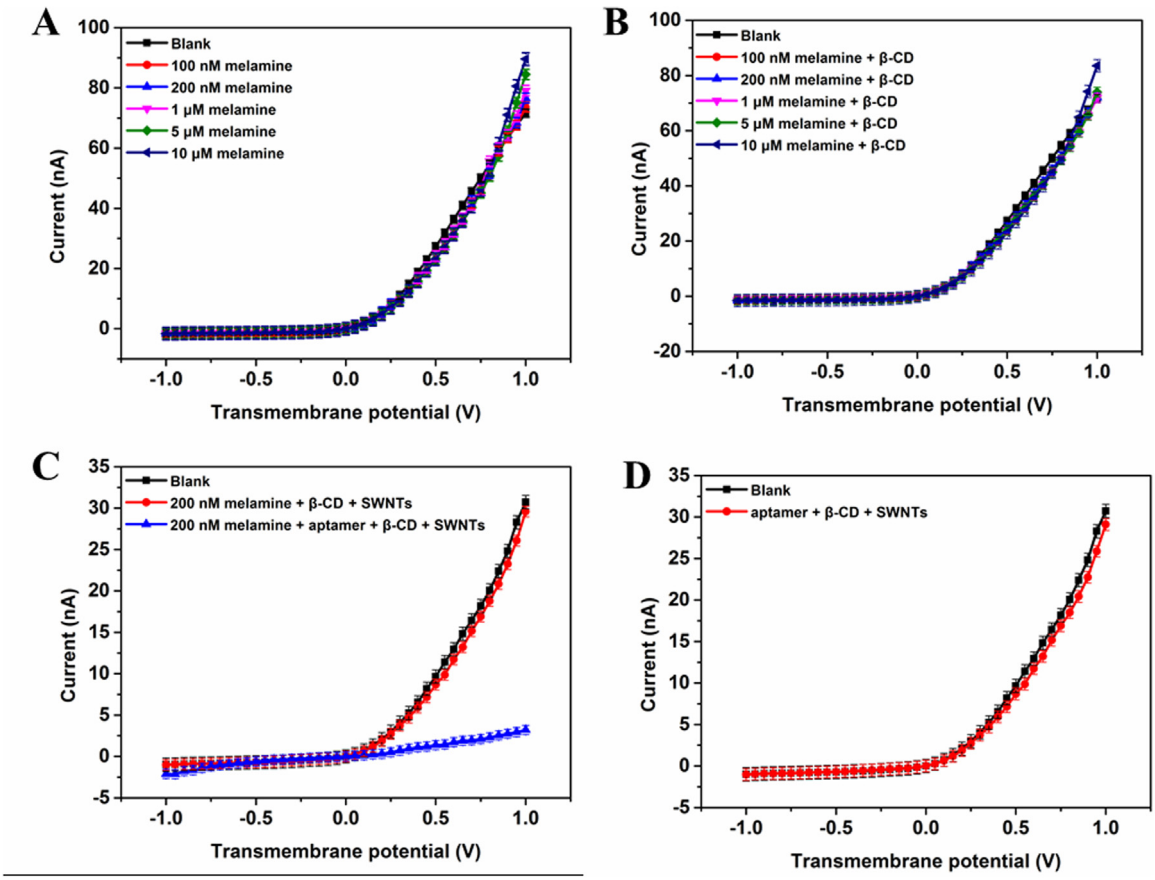

Fig. 1. Validation of the feasibility of the ICR biosensor: addition of cyclodextrin and SWNTs to eliminate the effect of excessive melamine and aptamer. Response of PEI/Zr^{4+}-modified conical nanofluidic channel to increasing melamine concentration before (A) and after (B) addition of cyclodextrin in the solution (tip diameter = 63 nm, base diameter = 1060 nm). (C) The presence of SWNTs eliminates the adsorption of the aptamer on the nanochannel surface modified with PEI/Zr^{4+} and (D) the coexistence of the aptamer and melamine induces a considerable change in current-voltage curve of the modified asymmetric nanochannel (tip diameter = 51 nm, base diameter = 1060 nm). Experimental conditions: aptamer of 200 nM, a buffering solution of 100 mM KCl and 10 mM tris-HCl at pH = 7.4, SWNTs of 50 μg/mL, 1 mM of β-CD.

relevant experimental conditions. To make sure the sensor is effective, there needs to be no signal variation in the absence or excess of target molecules. Unfortunately, as shown in Fig. 1**A,** the current increased with increasing melamine concentration. Thus, melamine could be adsorbed onto the outmost layer (Zr^{4+}) by a coordination interaction between the amino-group and Zr^{4+} in the absence of β-CD. However, the special interaction between the phosphate group and Zr^{4+} is very important for adsorption of dsDNA (Fig. S3A). To solve this problem, we added different ratios of β-CD into the melamine solution, since β-CD has been confirmed to effectively capture small molecules such as melamine, due to the host–guest inclusion of melamine into the hydrophobic cavity of β-CD (Fig. 1**B**). The shielding effect of β-CD was distinct when the ratio of β-CD to melamine was more than 200, which is reflected by the negligible current variation at large voltage (1 V).

One critical requirement of this ICR biosensor is the selective adsorption of dsDNA instead of ssDNA. Therefore, the free ssDNA has to be removed before interacting with the nanochannel surface. Since SWNTs have been confirmed to be excellent absorbents for ssDNA, we tested their effectiveness. As shown in Fig. 1**C**, a mixture of the aptamer, β-CD, and SWNTs was used in the electrochemical tests to determine that there was no significant change in the current. This confirmed that ssDNA can successfully interact with SWNTs without being disturbed by the addition of β-CD. In addition, the aptamer plays an important role in the detection of melamine. As shown in Fig. 1**D**, upon addition the aptamer, the biosensor clearly showed excellent detection capability to melamine. The optimal ratio of SWNTs to aptamer was determined when more than 93.5% of the FAM fluorescence grafted to ssDNA was quenched (Fig. S4). Without otherwise specified, this study used 50 μg/mL of SWNTs in the presence of 200 nM of aptamer for free aptamer elimination.

3.3. CD spectra and UV–vis absorption spectra of T36-DNA binding with melamine

To reconfirm that melamine can induce duplex formation, we further investigated the binding of T_{36}-DNA with melamine via a combination of UV–vis spectra and CD spectra. In the presence of melamine, it was experimentally confirmed that ssDNA forms dsDNA via hydrogen bonding between thymine and melamine (Stanly John Xavier, 2014). Fig. 2**A** shows the UV absorption spectra of T_{36}-DNA before and after the addition of melamine. The optical density decreased upon the addition of melamine, indicating the transition into a secondary structure of aptamers (Miyake et al., 2006). It was observed that circular dichroism (CD) spectra with a stronger CD signal at 280 nm shows palpable structural changes of T_{36}-DNA in the presence of melamine (Fig. 2**B**). Therefore, the results very well reproduced the features of melamine-induced duplex formation.

3.4. Confirmation of PEI and Zr^{4+} coating by XPS characterization

To further determine the modification of the nanochannel, X-ray photoelectron spectroscopy (XPS) was performed. The wide energy XPS spectrum showed that a much higher value for the N 1s peak at 399.6 eV appeared for the PEI-modified membrane (Fig. S5A), and

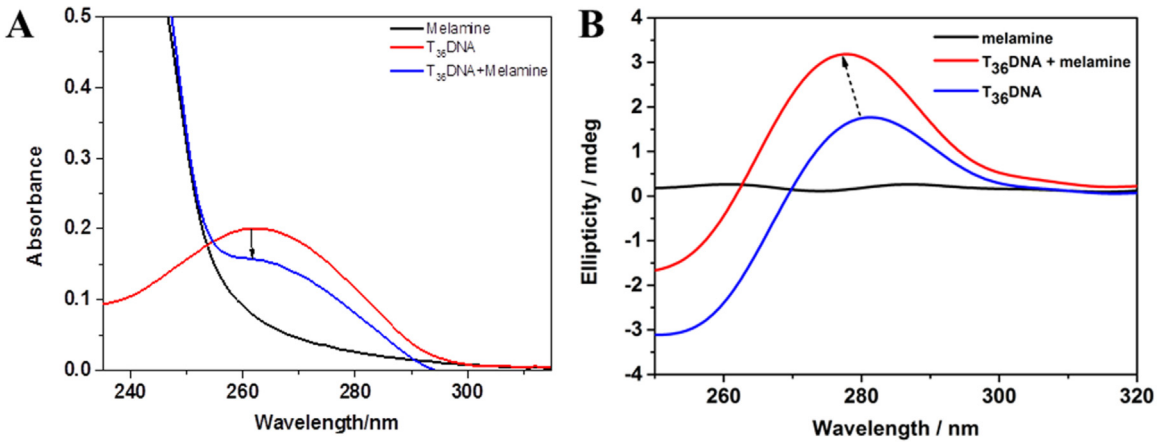

Fig. 2. Confirmation of the melamine-mediated formation of dsDNA. (A) The UV–vis absorption spectra of 200 nM T_{36}-DNA in Tris-HCl buffer (pH = 7.4) prior to and after the addition of 4 mM melamine; (B) The CD spectra of 1 μM T_{36}-DNA in the absence and presence of 4 mM melamine in Tris-HCl buffer (pH = 7.4).

peaks corresponding to Zr ($3d_{3/2}$ at 182.35 eV; $3d_{5/2}$ at 184.70 eV) were observed after completing the Zr^{4+}-modified process (Fig. S5B).

3.5. Quantitative analysis of melamine

The concentration of melamine determines the complex (melamine/aptamer) concentration, which can be monitored by the current-voltage curve. The PEI/Zr^{4+}-modified conical nanofluidic channel is positively charged, but the complex with a highly negative charged phosphate can effectually neutralize the positive charge of the nanochannel via electrostatic force. The change in the surface charge of the nanopore can be visibly monitored by the current-voltage curve. Therefore, the melamine concentration can be indirectly quantitated by the proposed platform. The adsorption behaviour of the complex follows the Langmuir absorption model. The melamine concentration was indirectly monitored by the variation of the current-voltage curve after the adsorption of the complex onto the surface of the nanochannel.

We used the Langmuir adsorption Eq. (1) and (2) to analyse the current data:

$$\theta = \frac{KC}{1 + KC} \quad (1)$$

where θ is the fractional coverage of the molecule on the sensor surface, K is the binding constant in units of L mol^{-1} and C is the concentration of melamine. θ is also given as follows:

$$\theta = (I_0 - I_i)/(I_0 - I_{min}) \quad (2)$$

where I_0 is the current obtained in the absence of melamine, I_i is defined as the corresponding ion current exposed to the solution. Additionally, Imin is the minimum current after the sensor surface is saturated by the highly concentrated complex (melamine/aptamer).

We used the current data at + 1 V, and a series of θ were obtained. A plot of the surface coverage (θ) versus concentration of melamine is shown in Fig. 3**B**, and the experimental data was fitted well according to Eq. (1).

Fig. 3**A** shows the gradual shift of the current-voltage curves in the presence of different concentrations of melamine from 0 nM to 5 μM in the buffer solution. By utilizing equation (3), the surface coverage (θ) could be derived. Upon plotting the surface coverage versus the melamine concentration, a proper calibration curve was obtained (Fig. 3**B**). The inset in Fig. 4B shows a linear relationship between the target melamine concentration and θ was observed in the wide concentration range of 0–200 nM for melamine. The linear regression equation was $y = 0.0263 + 4.52 * 10^{-3}$ Cmelamine ($R^2 = 0.9876$). Because sensitivity is defined as the slope of the standard curve, the value of biosensor sensitivity was $4.52 * 10^{-3}$ nM^{-1} according to the linear equation. The limit of detection (LOD) of the sensor could be calculated by the formula, LOD = 3σ/slope, where σ is the standard deviation of a blank solution, and the value of σ is 0.0065 in this study. As shown in Table S1, this biosensor exhibited a detection limit as low as 4.3 nM, which is better than many existing melamine sensors.

3.6. Specificity of the biosensor towards melamine

To evaluate the selectivity of the fabricated biosensor, interfering substances such as Cu^{2+}, Zn^{2+}, Fe^{3+}, Mg^{2+}, Ca^{2+}, ascorbic acid (Vc), glucose, and structural analogues of melamine (cyanuric acid), were selected for the test. Under the same experimental conditions, the I-V curve was acquired (Fig. 4**A**). As shown in Fig. 4**B**, adding most of the substances in dairy products and analogues of melamine only caused a slight ICR change. When the nanochannel interacted with melamine, the ICR change considerably increased. These data indicate that the PEI/Zr^{4+}-modified conical nanofluidic channel biosensor can distinguish melamine from interfering substances, exhibiting a desirable specificity.

3.7. Analysis of melamine in milk samples

To evaluate the feasibility of the biosensor in real samples, different concentrations of melamine were spiked into treated milk samples. Recovery experiments were used to evaluate the accuracy of our detection system. The current corresponding to a voltage of 1 V was measured as described above; then, the concentration of melamine could be calculated by using the above calibration curve. As shown in Table 1, the recovery was acquired from 97% to 112% with an RSD (n = 3) between 3.12% and 4.26%, showing a satisfactory result. Thus, the fabricated biosensor may be a competitive candidate for melamine determination in actual samples with an acceptable accuracy.

3.8. The reproducibility and stability of the conical nanofluidic channel biosensor

The biosensor exhibited good reproducibility and stability, which was demonstrated by repeated etching, modification and detection. Upon immersion in the aptamer, the current through the nanochannel was considerably reduced and short-time etching with 2 M NaOH for 5 min was good enough to remove the aptamer from the surface (Fig. S6A). When the nanochannel was modified, the current again increased. Reversible variation of the ionic current of the nanochannel at 1 V for four cycles reflected the high repeatability and stability of the system (Fig. S6B). We observed that repeated etching could gradually enlarge the nanochannel size; thus, long-term recycling of this

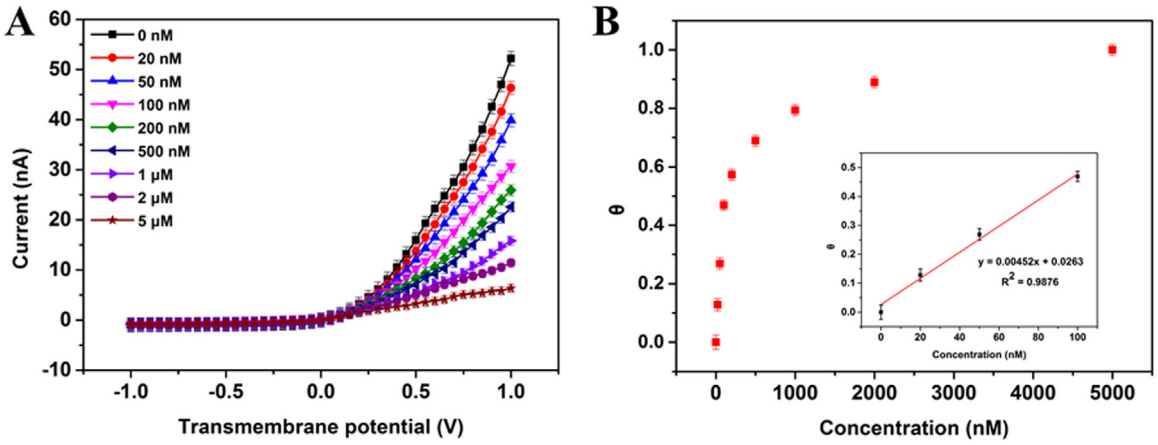

Fig. 3. Quantitative analysis of melamine based on the proposed biosensor. (A) I-V characteristics of the PEI/Zr4 + modified nanochannel (tip diameter = 51 nm, base diameter = 1060 nm) to different concentrations of melamine in the presence of 200 nM aptamer, 50 μg/mL of SWNTs and 1 mM β-CD. (B) Comparison of the surface coverage (θ) recorded at 1 V using different concentration of target melamine in the designed platform.

biosensor is not recommended.

4. Conclusions

In conclusion, a biosensor based on a single nanochannel for highly sensitive and selective melamine recognition was fabricated by utilizing β-cyclodextrin to eliminate the absorption of free melamine on the nanochannel via a the host-guest interaction, and using SWNTs to remove interfering ssDNA, respectively. The biosensor showed a wide detection range, a low detection limit and a good selectivity towards melamine over other interfering substances. Compared with the previously reported methods for melamine quantification, this approach is highly sensitive, easy to operate and quite efficient. In future research, this strategy could be further used to evaluate extensive ranges of targets due to the flexibility of replacing the corresponding aptamer. Furthermore, a variety of supramolecules could be used to effectively eliminate the effects of interfering substances via host-guest interactions, thus providing a versatile and universal platform for target detection in real samples with a preferable selectivity and sensitivity.

Acknowledgements

This work was supported by the National Natural Science Foundation of China (Nos. 21575078, 21676060 and 21472143) and the Major Project of Collaboration and Innovation of Guangzhou City, University and Research Institute (201704020005).

Table 1
Application of the proposed method for the detection of melamine in real samples.

Sample	Added (nM)	Found (nM)	Recovery (%)	RSD (n = 3, %)
Liquid Milk	0	0		
1	20	22.4	112	4.26
2	50	48.5	97	3.12
3	100	108.2	108.2	3.38

Declaration of interest statement

We declare that we have no financial and personal relationships with other people or organizations that can inappropriately influence our work, there is no professional or other personal interest of any nature or kind in any product, service and/or company that could be construed as influencing the position presented in, or the review of, the manuscript entitled.

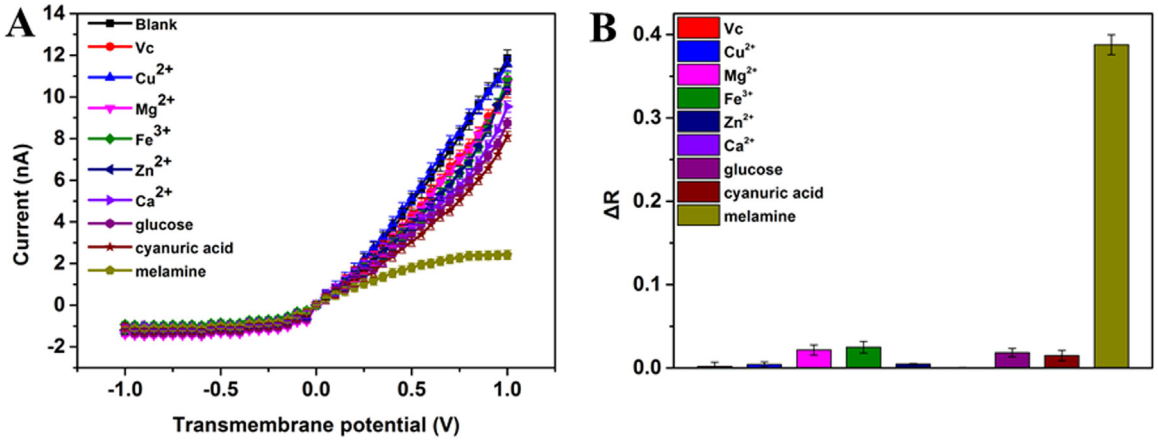

Fig. 4. Specificity of this assay for melamine detection against cyanuric acid and coexisting substances that potential exist in dairy products. (A) The responses of the biosensor (tip diameter = 44 nm, base diameter = 1060 nm) to Cu^{2+}, Zn^{2+}, Fe^{3+}, Mg^{2+}, Ca^{2+}, ascorbic acid (Vc), glucose cyanuric acid and melamine, respectively, in the presence of 200 nM aptamer, 50 μg/mL of SWNTs and 1 mM of β-CD. (B) Column chart corresponding to (A) via the ICR change ($\Delta R = Ri - R0 = \frac{I_i(-1)}{I_i(+1)} - \frac{I_0(-1)}{I_0(+1)}$) of the modified nanochannel in the presence of 100 nM concentration of the abovementioned substances, where Ri is the ICR at a concentration of 100 nM for each subject, and R0 is the ICR for a blank buffering solution.

Appendix A. Supplementary material

Supplementary data associated with this article can be found in the online version at doi:10.1016/j.bios.2018.12.020.

References

Ahmad, S.A., Ahmed, M., Qadir, M.A., Shafiq, M.I., Batool, N., Nosheen, N., Ahmad, M., Mahmood, R.K., Khokhar, Z.U., 2016. Food Anal. Method. 9 (12), 3367–3376.
Ai, K.L., Lu, L.H., 2009. J. Am. Chem. Soc. 131, 9496–9497.
Bai, W., Kuang, T., Chitrakar, C., Yang, R., Li, S., Zhu, D., Chang, L., 2018. Biosens. Bioelectron. 122, 189–204.
Balabin, R.M., Smirnov, S.V., 2011. Talanta 85 (1), 562–568.
Beamish, E., Tabard-Cossa, V., Godin, M., 2017. ACS Sens. 2 (12), 1814–1820.
Boussouar, I., Chen, Q., Chen, X., Zhang, Y., Zhang, F., Tian, D., White, H.S., Li, H., 2017. Anal. Chem. 89 (2), 1110–1116.
Chen, D., Zhao, Y., Miao, H., Wu, Y., 2015. Talanta 134, 144–152.
Chen, Q., Rozovsky, S., Chen, W., 2017. Chem. Commun. 53 (54), 7569–7572.
Chen, Y., Zuo, Z., Dai, X., Xiao, P., Fang, X., Wang, X., Wang, W., Ding, C.F., 2018. Talanta 186, 1–7.
Chi, X., Ji, X., Xia, D., Huang, F., 2015. J. Am. Chem. Soc. 137 (4), 1440–1443.
Creamer, J.S., Mora, M.F., Willis, P.A., 2018. Electrophoresis.
Diao, W., Tang, M., Ding, S., Li, X., Cheng, W., Mo, F., Yan, X., Ma, H., Yan, Y., 2018. Biosens. Bioelectron. 100, 228–234.
Domingo, Ed.C., Tireli, A.A., Nunes, C.A., Batista, A.V., Guerreiro, M.C., Pinto, S.M., 2015. Talanta 132, 535–540.
Fang, C., Ji, H., Karen, W.Y., Rafei, S.R.M., 2011. Biosens. Bioelectron. 26 (5), 2670–2674.
Ge, X., Wu, X., Wang, J., Liang, S., Sun, H., 2015. J. Dairy. Sci. 98 (4), 2161–2171.
Giovannozzi, A.M., Rolle, F., Sega, M., Abete, M.C., Marchis, D., Rossi, A.M., 2014. Food Chem. 159, 250–256.
Guo, H., Zhou, X., Zhang, Y., Song, B., Liu, L., Zhang, J., Shi, H., 2014. Sens. Actuators B-Chem. 194, 114–119.
Guo, Z., Gai, P., Hao, T., Wang, S., Wei, D., Gan, N., 2011. Talanta 83 (5), 1736–1741.
Guo, Z., W, J.H., Wang, E.K., 2012. Talanta 89, 253–257.
Han, S., Zhu, S., Liu, Z., Hu, L., Parveen, S., Xu, G., 2012. Biosens. Bioelectron. 36 (1), 267–270.
Hanson, K.L., Fulga, F., Dobroiu, S., Solana, G., Kaspar, O., Tokarova, V., Nicolau, D.V., 2017. Biosens. Bioelectron. 93, 305–314.
Hardy, A., Seguin, C., Brion, A., Lavalle, P., Schaaf, P., Fournel, S., Bourel-Bonnet, L., Frisch, B., De Giorgi, M., 2018. ACS Appl. Mater. Interfaces 10 (35), 29347–29356.
Hu, H., Zhang, J., Ding, Y., Zhang, X., Xu, K., Hou, X., Wu, P., 2017. Anal. Chem. 89 (9), 5101–5106.
Hu, R., Rodrigues, J.V., Waduge, P., Yamazaki, H., Cressiot, B., Chishti, Y., Makowski, L., Yu, D., Shakhnovich, E., Zhao, Q., Wanunu, M., 2018. ACS Nano 12 (5), 4494–4502.
Huang, H., Li, L., Zhou, G., Liu, Z., Ma, Q., Feng, Y., Zeng, G., Tinnefeld, P., He, Z., 2011. Talanta 85 (2), 1013–1019.
Huang, Y., Tian, K., Min, S., Xiong, Y., Du, G., 2015. Food Chem. 177, 174–181.
Idili, A., Ricci, F., Vallee-Belisle, A., 2017. Nucleic Acids Res. 45 (13), 7571–7580.
Ji, Yl, Chen, Xw, Zhang, Zb, Li, J., Xie, Ty, 2014. J. Sep. Sci. 37 (20), 3000–3006.
Jiang, Y., Pan, X., Chang, J., Niu, W., Hou, W., Kuai, H., Zhao, Z., Liu, J., Wang, M., Tan, W., 2018. J. Am. Chem. Soc. 140 (22), 6780–6784.
Kong, Y., Wei, C., Hou, Z., Wang, Z., Yuan, J., Yu, J., Zhao, Y., Tang, Y., Gao, M., 2014. J. Anal. Methods Chem. 2014, 212697.
Lee, J., Jeong Jeong, E., Kim, J., 2011. Chem. Commun. 47 (1), 358–360.
Li, J., Geng, S., Liu, B., Wang, H., Liang, G., 2018. Food Res. Int. 112, 136–142.
Li, W., Meng, M., Lu, X., Liu, W., Yin, W., Liu, J., Xi, R., 2013. Food Agr. Immunol. 25 (4), 498–509.
Liang, X., Wei, H., Cui, Z., Deng, J., Zhang, Z., You, X., Zhang, X.E., 2011. Analyst 136 (1), 179–183.
Liao, T., Li, X., Tong, Q., Zou, K., Zhang, H., Tang, L., Sun, Z., Zhang, G.J., 2017. Anal. Chem. 89 (10), 5511–5518.
Lin, Y., Shi, X., Liu, S.C., Ying, Y.L., Li, Q., Gao, R., Fathi, F., Long, Y.T., Tian, H., 2017a. Chem. Commun. 53 (25), 3539–3542.
Lin, Y., Ying, Y.L., Shi, X., Liu, S.C., Long, Y.T., 2017b. Chem. Commun. 53 (84), 11564–11567.
Meng, H.M., Fu, T., Zhang, X.B., Wang, N.N., Tan, W., Shen, G.L., Yu, R.Q., 2012. Anal. Chem. 84 (5), 2124–2128.
Miyake, Y.T., Humika, Tashiro, M., Yamaguchi, H., Oda, S.J., Kudo, M., Tanaka, Y., Kondo, Y., Sawa, R., Fujimoto, T., Machinami, T., Ono, A., 2006. J. Am. Chem. Soc. 128, 2172–2173.
Nagy, G., Chouinard, C.D., Attah, I.K., Webb, I.K., Garimella, S.V.B., Ibrahim, Y.M., Baker, E.S., Smith, R.D., 2018. Electrophoresis.
Niu, B., Xiao, K., Huang, X., Zhang, Z., Kong, X.Y., Wang, Z., Wen, L., Jiang, L., 2018. 7. ACS Appl. Mater. Inter. 10 (26), 22632–22639.
Ogoshi, T., Yamagishi, T.A., Nakamoto, Y., 2016. Chem. Rev. 116 (14), 7937–8002.
Qi, W., Zhao, J., Zhang, W., Liu, Z., Xu, M., Anjum, S., Majeed, S., Xu, G., 2013. Anal. Chim. Acta 787, 126–131.
Qian, Y., Zhang, Z., Kong, X.Y., Tian, W., Wen, L., Jiang, L., 2018. ACS Appl. Mater. Inter. 10 (36), 30852–30859.
Rajapandiyan, P., Tang, W.L., Yang, J., 2015. Food Control 56, 155–160.
Rani, R., Medhe, S., Srivastava, M., 2014. Dairy Sci. Technol. 95 (2), 257–263.
Shang, X., Xie, G., Kong, X.Y., Zhang, Z., Zhang, Y., Tian, W., Wen, L., Jiang, L., 2017. Adv. Mater. 29 (3), 1603884.
Song, S., Chong, Y., Fu, H., Ning, X., Shen, H., Zhang, Z., 2018. ACS Appl. Mater. Interfaces 10 (40), 33867–33878.
Sun, F.M., Xu, L.G., Zhu, Y.Y., Liu, L.Q., Peng, C.F., Wang, L.B., Kuang, H., Xu, C.L., 2010. Trac. Trend Anal. Chem. 29, 11.
Sun, Y., Guo, F., Zuo, T., Hua, J., Diao, G., 2016. Nat. Commun. 7, 12042.
Wang, B., Han, J., Bender, M., Hahn, S., Seehafer, K., Bunz, U.H.F., 2018a. ACS Sens. 3 (2), 504–511.
Wang, J., Hou, J., Zhang, H., Tian, Y., Jiang, L., 2018b. ACS Appl. Mater. Interfaces 10 (2), 2033–2039.
Wang, G.L., Jiao, H.J., Zhu, X.Y., Dong, Y.M., Li, Z.J., 2012. Talanta 93, 398–403.
Wang, T.T., Xuan, R.R., Ma, J.F., Tan, Y., Jin, Z.F., Chen, Y.H., Zhang, L.H., Zhang, Y.K., 2016. Anal. Bioanal. Chem. 408 (24), 6671–6677.
Wang, Y., Zhang, J., Zhu, L., Lu, L., Feng, C., Wang, F., Xu, Z., Zhang, W., 2015a. Analyst 140 (22), 7508–7512.
Wang, Y.S., Zhu, L.L., Zhang, J.Y., Wang, F.Y., Lu, L.L., Yu, H.J., Xu, Z.A., Zhang, W., 2015b. Chem. Commun. 51, 7958.
Wu, T., Chen, H., Lin, Z., Tan, C., 2016. J. Spectrosc. 2016, 1–8.
Xavier, Stanly John, S.K, C., Gnana kumar, G., Kimb, Ae. Rhan, Yoo, Dong Jin, 2014. Anal. Methods 6, 8165.
Xie, W., Huang, Y., Tang, D., Zhang, H., Du, C., Zhu, Y., Zhang, W., 2015a. J. Food Qual. 38, 297–304.
Xie, G.X., Zhang, Z., Kong, X.Y., Liu, Q., Li, P., Wen, Lp, Jiang, L., 2015b. Angew. Chem. Int. Ed. 54, 13664–13668.
Xue, M., Wei, W., Su, Y., Johnson, D., Heath, J.R., 2016. J. Am. Chem. Soc. 138, 3085–3093.
Yang, H., Lu, F., Sun, Y., Yuan, Z., Lu, C., 2018. Anal. Chem.
Yin, B., Xie, W., Liang, L., Deng, Y., He, S., He, F., Zhou, D., Tlili, C., Wang, D., 2017. ACS Omega 2 (10), 7127–7135.
Zeng, Y., Pratumyot, Y., Piao, X., Bong, D., 2012. J. Am. Chem. Soc. 134 (2), 832–835.
Zhai, Q., Zhang, S., Jiang, H., Wei, Q., Wang, E., Wang, J., 2014. J. Mater. Chem. B 2 (37), 6371–6377.
Zhang, J., Wu, M., Chen, D., Song, Z., 2011. J. Food Compos. Anal. 24 (7), 1038–1042.
Zhang, L., Li, T., Li, B., Li, J., Wang, E., 2010a. Chem. Commun. 46 (9), 1476.
Zhang, L., Wei, H., Li, J., Li, T., Li, D., Li, Y., Wang, E., 2010b. Biosens. Bioelectron. 25 (8), 1897–1901.
Zhang, S., Bao, A., Sun, T., Wang, E., Wang, J., 2015. Biosens. Bioelectron. 63, 287–293.
Zhao, X., Chen, L., 2016. J. Sep. Sci. 39 (19), 3775–3781.
Zheng, H., Li, X., Jia, Q., 2018. ACS Appl. Mater. Interfaces. 10 (23), 19914–19921.
Zhou, Y., Gao, L., Tong, X., Li, Q., Fei, Y., Yu, Y., Ye, T., Zhou, X.S., Shao, Y., 2018. Anal. Chem.
Zhu, L., Gamez, G., Chen, H., Chingin, K., Zenobi, R., 2009a. Chem. Commun. 5, 559–561.
Zhu, L., Zhao, Z., Zhang, X., Zhang, H., Liang, F., Liu, S., 2018a. Molecules 23 (4), 947.
Zhu, L., Xu, Y., Ali, I., Liu, L., Wu, H., Lu, Z., Liu, Q., 2018b. ACS Appl. Mater. Inter. 10 (31), 26555–26565.
Zhuang, H., Zhu, W., Yao, Z., Li, M., Zhao, Y., 2016. Talanta 153, 186–190.